# NASA TECHNICAL MEMORANDUM

NASA TM-78843




# BOUNDARY LAYER ANALYSIS OF A CENTAUR STANDARD SHROUD

by W. R. Hingst and C. E. Towne
Lewis Research Center
Cleveland, Ohio 44135

March 1978

| 1 Report No<br>NASA TM-78843 | 2 Government Accession No. | 3 Recipient's Catalog No |
|---|---|---|
| 4. Title and Subtitle<br>BOUNDARY LAYER ANALYSIS OF A CENTAUR STANDARD SHROUD | | 5 Report Date<br>March 1978<br>6. Performing Organization Code |
| 7. Author(s)<br>W. R. Hingst and C. E. Towne | | 8 Performing Organization Report No<br>E-9557<br>10. Work Unit No. |
| 9. Performing Organization Name and Address<br>National Aeronautics and Space Administration<br>Lewis Research Center<br>Cleveland, Ohio 44135 | | 11 Contract or Grant No. |
| 12. Sponsoring Agency Name and Address<br>National Aeronautics and Space Administration<br>Washington, D.C. 20546 | | 13. Type of Report and Period Covered<br>Technical Memorandum<br>14. Sponsoring Agency Code |

15. Supplementary Notes

16 Abstract

An analytical boundary layer investigation was carried out in conjunction with an experimental wind tunnel test to determine the discharge characteristics of the Centaur shroud ascent vent system on the Titan/Centaur launch vehicle. This involved estimating the effect of the local boundary layers on the vent discharge for vehicle Mach numbers ranging from 0.8 to 1.56. The growth of the boundary layer along the vehicle was influenced by the interaction with flanges protruding into the flow and by the longitudinal corrugations in the vehicle surface. The effects of the flange and corrugations were treated by approximate techniques. In addition, boundary layer calculations were made for a 3 percent model of the launch vehicle and compared with experimental results.

| 17 Key Words (Suggested by Author(s)) | 18 Distribution Statement |
|---|---|
| Boundary layers; Fluid flow; Transonic flow; Approximate solutions; Control volume methods | Unclassified - unlimited<br>STAR Category 34 |

| 19 Security Classif (of this report) | 20 Security Classif (of this page) | 21 No of Pages | 22 Price* |
|---|---|---|---|
| Unclassified | Unclassified | | |

*For sale by the National Technical Information Service, Springfield, Virginia 22161

# BOUNDARY LAYER ANALYSIS OF A CENTAUR STANDARD SHROUD

by W. R. Hingst and C. E. Towne

Lewis Research Center

E-9557

## SUMMARY

An analytical boundary layer investigation was carried out in conjunction with an experimental wind tunnel test to determine the discharge characteristics of the Centaur shroud ascent vent system on the Titan/Centaur launch vehicle. This involved estimating the effect of the local boundary layers on the vent discharge. The growth of the boundary layer along the vehicle was influenced by the interaction with flanges protruding into the flow over the body and by the longitudinal corrugations in the vehicle surface. In addition, boundary layer calculations were made for a 3 percent modal of the launch vehicle, and were compared with experimental results. The effect of the flange interacting with the boundary layer was determined using a control volume technique. The calculation of boundary layer growth over the corrugations was estimated by using a surface roughness in the boundary layer calculations that would simulate the effect of the corrugations. Calculations were made for both the vehicle and model for Mach numbers ranging from 0.8 to 1.56. A comparison of analytical results with experimental data shows very good agreement for the supersonic Mach numbers. At the lower Mach numbers the agreement between experiment and analysis was not as good.

# INTRODUCTION

During preparation for the Titan/Centaur-Viking proof flight, it was necessary to verify the adequacy of the Centaur shroud ascent vent system on the Titan/Centaur launch vehicle. The ascent vent system was designed to vent the internal air of the shroud during the ascent phase of the mission to prevent significant pressure loading on the vehicle. The problem essentially resolved itself into the ability to estimate the correct discharge coefficient for the vents while the vehicle was in the transonic flight regime. This involved estimating the effect of the local boundary layer on the vents. The growth of the boundary layer along the vehicle was influenced by the interaction with flanges protruding into the flow over the body and longitudinal corrugations in the vehicle surface.

To determine these discharge coefficients, a series of tests were conducted in the Lewis 8×6 foot supersonic wind tunnel (ref. 1). Since it was impractical to test the full scale vehicle in the wind tunnel, the boundary layers that the vents would see in free flight were calculated, and these boundary layers were artifically produced in the wind tunnel using thickening devices. The discharge coefficients of the full scale vents were then determined using these artifically thickened boundary layers in the wind tunnel test. In addition, tests were conducted on a 3 percent Centaur shroud model. These tests measured the pressure distribution on the model, especially in the vicinity of the flanges, and determined the effect of the flanges on the boundary layer. Calculations similar to those made for the full scale Centaur shroud were needed for the 3 percent model to estimate the boundary layer height. From these results the flange on the 3 percent model was scaled to the boundary layer thickness rather than geometrically. That is, the flanges on the 3 percent model extended into the boundary layer the same fraction of the boundary layer thickness as the flanges on the full scale vehicle.

This study reports calculations that were made to predict the boundary layer parameters along the Centaur launch vehicle and the 3 percent model in the transonic flight regime. The analysis included calculations

of the laminar boundary layer, estimations of the laminar-turbulent transition locations and calculations of the turbulent boundary layers. In addition, a separate analysis was required to determine the effect of the flange on the boundary layer, and the longitudinal corrugations in the vehicle surface had to be taken into account. The analysis used to calculate the boundary layer for the 3 percent model was similar to that used for the full scale vehicle. However, the 3 percent model did not have the corrugated surface.

Calculations for both the full scale vehicle and 3 percent model were made for Mach numbers between 0.8 and 1.56. From the flight schedule of the vehicle the free stream static pressure at Mach 0.8 was $6.1504 \times 10^4$ N/m$^2$ and at Mach 1.56 was $2.4318 \times 10^4$ N/m$^2$. Since the results of the testing and therefore the analysis were needed before the proof flight, little time was available for development of elaborate analytical techniques. Therefore, techniques that were available or could be quickly devised were used in the analysis. Figures 1(a) to 1(c) show the dimensions of the vehicle and the dimensions and locations of the flange and surface corrugations. The approximate methods used here for the effect of the corrugations and flanges on the boundary layer could be applied to similar problems in other areas.

## METHOD OF ANALYSIS

The boundary layer properties were calculated using the finite difference computer program of reference 2 and a finite difference computer program based on the turbulence model of reference 3. The two computer programs gave essentially the same results. Both the laminar and turbulent boundary layer properties were calculated with these programs using the appropriate viscosity. The transition location was estimated to occur during the first adverse pressure gradient on the nose of the vehicle and at the shoulder of the 3 percent model, figure 1. As would be expected, when dealing with a body the size of the full scale vehicle, the results at the downstream locations near the vents were not particularly sensitive to the choice of any reasonable transition loca-

tion. On the 3 percent model the comparison of the boundary layer parameters with the test results served as a indirect check on the transition location estimation. The boundary layer analysis did not include a separate shock-boundary layer analysis but calculated the properties by smoothing the surface pressure distribution through the interaction region to the extent that the boundary layer program could be used through the interaction region.

For the areas of the Centaur shroud with the corrugated surface, figure 1, a method was needed to determine the effect of the surface on the growth of the boundary layer. The problem is a three dimensional one. Because of the need for immediate results, however, an effort was made to estimate the effect of the corrugations rather than attempt a more rigorous three dimensional analysis. The technique used in this study to estimate the effect of the corrugations was to determine an equivalent surface roughness that would cause the same thickening of the boundary layer as the corrugations. The boundary layer program described in reference 2 was capable of calculating the boundary layer properties for a surface that could be described by an equivalent sand roughness. The ratio of the actual corrugated surface area to projected area was determined from the geometry of the corrugations. It was then assumed that the skin friction would increase by approximately the same amount. Therefore, from the relationship between sand roughness and local skin friction presented in reference 4 for flat plates, an equivalent sand roughness was determined and used in the boundary layer program. To summarize, the effect of corrugations on the boundary layer was estimated by assuming that an equivalent sand roughness could be determined that would approximate the effect of the corrugations.

The effect of the flange interacting with the boundary layer had to be determined independently. The boundary layer program was terminated at the flange, the effect of the flange on the boundary layer was then calculated, and the boundary layer program restarted using the boundary layer properties determined from the interaction analysis. The method used to determine the influence of the flange was essential-

ly a control volume analysis. In this approach, the details of the flow in the interaction region are not considered. The boundary layer properties downstream of the interaction region are determined from the upstream properties by using conservation of mass and momentum across the interaction region. In this analysis, it is assumed that in the interaction region the loss in momentum as a result of the boundary layer interacting with the flange is sufficiently large that other losses in momentum may be neglected. Therefore, the interaction analysis primarily involves obtaining an estimate of the drag on the flange and, from this value of drag, obtain the change in momentum of the boundary layer through the interaction region.

The drag coefficient for the flange was determined using a somewhat different technique for the supersonic and subsonic cases. For the subsonic cases, the drag coefficient was determined from empirical results, such as those in reference 5, for rectangular bodies at the average Mach number seen by the flange. For cases where the local flow was supersonic, the drag coefficient for the flange was determined using the average Mach number determined not from the undisturbed local boundary layer but from the Mach number that would occure behind an oblique shock seeing the local edge conditions. This modification for the supersonic cases was used because for supersonic flow a separation region is produced upstream of the flange. For this situation the shock shape produced by the flange would be more accurately described as resulting from a wedge than a rectangular body. The assumption here is that the drag behavior is similar to the well known reduction in drag experienced by a blunt body in supersonic flow when a spike is added to the nose, or in a two-dimensional case, when a thin protruding plate is added to a thick plate. In the analysis under consideration, the vehicle surface acts as the protruding plate. In calculating the drag for the supersonic cases, the extent of the separation region upstream of the flange was estimated from an empirical correlation given in reference 6. From this information the amount of flow turning and the oblique shock strength were determined. The edge Mach number was then calculated from conditions behind the oblique shock and this Mach

number was used as in the subsonic cases for determining the drag on the flange.

After determining the drag on the flange, the boundary layer downstream of the interaction is determined from the incoming flow condition and the value of the flange drag. The boundary layer calculations were then restarted using an essentially equilibrium boundary layer with the momentum defect calculated from the interaction analysis. No attempt was made to determine the exact details of the boundary layer flow in the separation and reattachment regions immediately upstream and downstream of the flange.

## DISCUSSION OF RESULTS

### Vehicle Boundary Layer

The boundary layer analysis for the full scale Centaur shroud vehicle was made at four vehicle Mach numbers, 0.8, 0.9, 1.0 and 1.56. The free stream static pressure and temperature vs. the vehicle Mach number for the vehicle flight schedule is presented in figure 2. This shows the decrease in static pressure and temperature with the increase in speed and altitude. In figures 3(a) to (e) the pressure coefficient on the vehicle body is given for five Mach numbers as a function of vehicle length. This was obtained from a potential flow analysis with no flanges. From this information the input parameters are determined for calculation of the boundary layer properties.

Figures 4(a) to (d) show the results of the boundary layer analysis and the control volume approach for analyzing the boundary layer-flange interaction. Shown on the figures are the boundary layer displacement thickness vs. the longitudinal position along the vehicle. The step change in the displacement thickness corresponds to the location of the flange on the vehicle.

Figure 5 shows the comparison of the analysis with the results of the wind tunnel experiments reported in reference 1. The data on this plot represent measurements taken on the wind tunnel wall using a full

scale model of the flange. The boundary layer upstream of the flange was generated to duplicate the full scale boundary layer predicted by the analysis. The downstream displacement thickness is compared at various freestream Mach numbers. There results show a fair agreement between the analysis and the experimental measurements. The largest difference in the comparison occurs at the lower Mach numbers. As discussed in the Method of Analysis section, determination of the flange drag coefficient for modeling the boundary layer interaction at the lower Mach numbers may have contributed to the inaccuracies in the calculations. From examining the results of the Mach 1.56 case, the assumption of a wedge-like interference for the flange in cases of supersonic flow seemed to predict the interaction correctly.

## 3 Percent Model Boundary Layer

The boundary layer analysis for the 3 percent model was made at four Mach numbers: 0.8, 1.0, 1.2 and 1.56. The model contours and pressure distributions were obtained from figures 1 and 3 using the appropriate scaling for the model dimensions. Boundary layer calculations were first made for the model without the rings that simulated the flanges on the full scale vehicle. The results of these calculations are shown in figures 6(a) to (d) as continuous lines. The plots show the displacement thickness as a function of longitudinal distance along the model. Also on the plots are the boundary layer measurements taken on the model in the wind tunnel tests. The agreement between the analysis and the data is very good at the supersonic Mach numbers but it deteriorated at the lower Mach numbers. This loss in accuracy at transonic Mach numbers could result from disturbances feeding forward from the solid rocket boosters that were located just downstream of the boattail section of the shroud. The boundary layer analysis would not account for this upstream influence.

Also shown on figure 6 are the analytical and experimental results for the 3 percent model with a 0.047 cm high ring to simulate the effect of the full scale vehicle flange. The 0.047 cm height of the ring re-

presents the fraction of the boundary layer on the model equivalent to the distance the flange extends into the boundary layer on the vehicle. For this case the boundary layer growth up to the ring is the same as in the no ring configuration. A step change in the boundary layer thickness parameters is shown at the ring location. The results of the boundary layer calculations are then shown to the aft of the model where the analysis is compared with the results of the wind tunnel measurements. Here, as in the case without the rings in place; the comparison is better at the supersonic Mach numbers than at the lower Mach numbers. The good agreement between the analysis and measurements at the forward probe location indicates that the laminar-turbulent transition location was predicted correctly.

An even more critical comparison between the boundary layer analysis and the experimental wind tunnel measurements can be made by comparing the predicted and measured boundary layer profiles. Figures 7 to 10 show the calculated boundary layer velocity profiles along with the measured values for the four Mach numbers under consideration. These plots show the excellent agreement at the supersonic Mach numbers. The difference between the analytical and measured profiles at the lower Mach numbers occurs in the outer portion of the boundary layer. These results are consistent with the suggestion that the measured profiles are being distorted by some transonic flow interaction on the model at these Mach numbers. It should be noted that there is a change in the scale of the ordinate between the forward boundary layer profiles and the aft profiles. The thickness of the aft boundary layer profiles is approximately twice that of the forward profiles.

## SUMMARY OF RESULTS

To estimate the boundary layer properties over vents on the standard Centaur shroud, boundary layer analyses were used that utilized approximate techniques to include the effects of flange-boundary layer interactions and longitudinal surface corrugations. Calculations were made for the full scale vehicle, a 3 percent wind tunnel model and a full

scale portion of the shroud tested in the wind tunnel. Comparisons between wind tunnel data and analysis indicated:

1. The results of the full scale vehicle calculations show good agreement with the boundary layer measurements downstream of the flange for supersonic flow but gave smaller displacement thicknesses than the experimental data for the subsonic free stream cases.

2. Comparison of the 3 percent model calculations with the wind tunnel data show a trend similar to that of the full scale flange wind tunnel data, that is, good agreement at supersonic Mach numbers with less agreement for the aft boundary layer location for the subsonic Mach numbers.

3. The overall results show that the approximate boundary layer techniques described here could be used in other similar problems, where the exact details of the boundary layer flow in the flange interaction region are not needed.

## APPENDIX - SYMBOLS

Cp pressure coefficient = $\dfrac{p - p_\infty}{\frac{1}{2}\rho_\infty u_\infty^2}$

M Mach number

p static pressure

r radius

t static temperature

u local flow velocity

x axial distance

y distance normal to surface

$\rho$ fluid density

$\delta^*$ boundary layer displacement thickness

Subscripts:

e boundary layer edge

r sea level

$\infty$ free stream

## REFERENCES

1. Johns, Albert L.; and Jones, Merle L.: Wind Tunnel Investigation of a Centaur Standard Shroud Compartment Vent from Mach Number of 0.70 to 1.96. NASA TM X-71759, 1975.

2. McDonald Henry; and Fish, R. W.: Practical Calculations of Transitional Boundary Layers. Int. J. Heat Mass Transfer, vol. 16, no. 9, Sep. 1973, pp. 1729-1744.

3. Herring, James H.; and Mellor, George L.: A Method of Calculating Compressible Turbulent Boundary Layers. NASA CR-1144, 1968.

4. Schlichting, Hermann (J. Kestin, transl.): Boundary Layer Theory. Fourth ed. McGraw-Hill Book Co., Inc., 1960, pp. 551-557.

5. Hoerner, Sighard F.: Fluid-Dynamic Drag. Second ed. Published by the Author, 1958, pp. 16-13 to 16-16.

6. Chang, Paul K.: Separation of Flow. Pergamon Press, 1970, pp. 272-335.

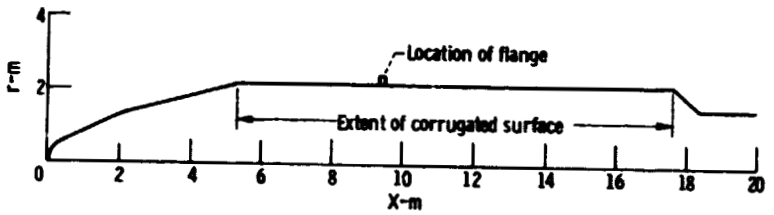


(a) Profile of Titan/Centaur vehicle shroud.

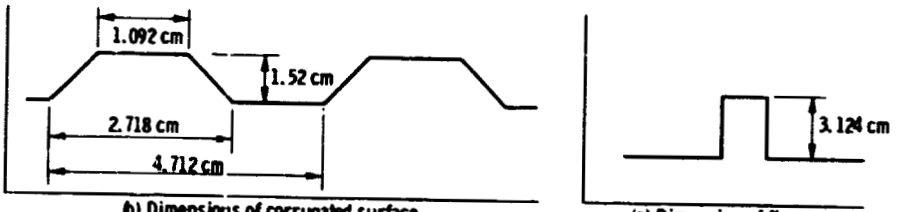


(b) Dimensions of corrugated surface.

(c) Dimension of flange.

Figure 1.

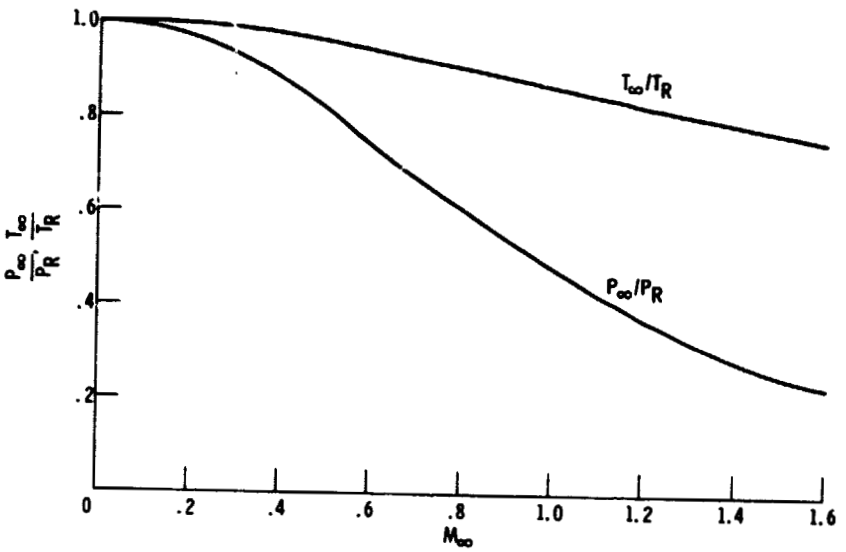


Figure 2. - Free stream static pressure and temperature vs vehicle Mach number.

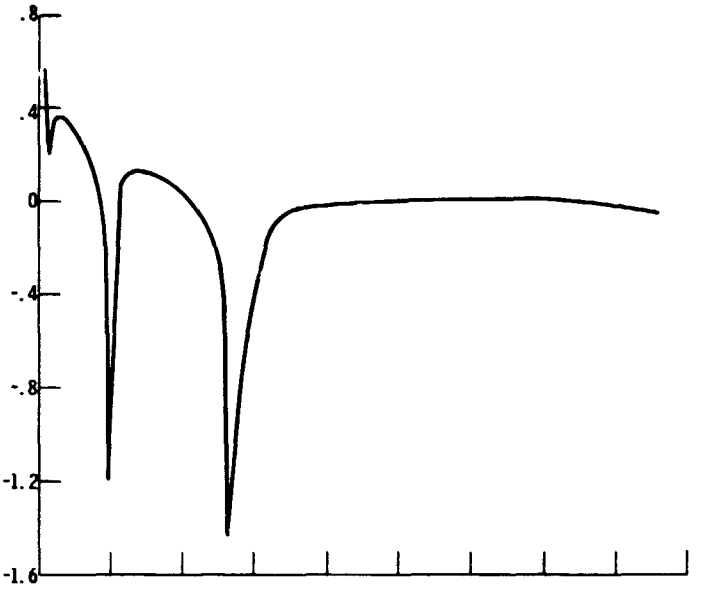


(a) Surface pressure coefficient vs distance along vehicle at $M_\infty = 0.8$.

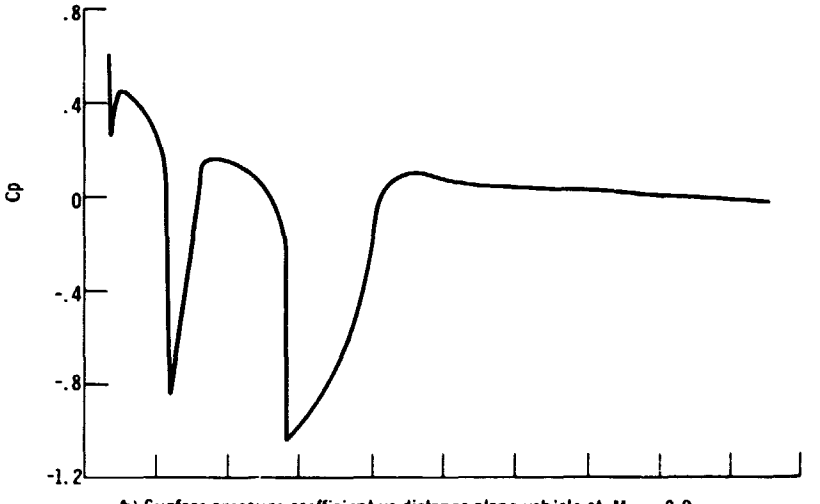


(b) Surface pressure coefficient vs distance along vehicle at $M_\infty = 0.9$.

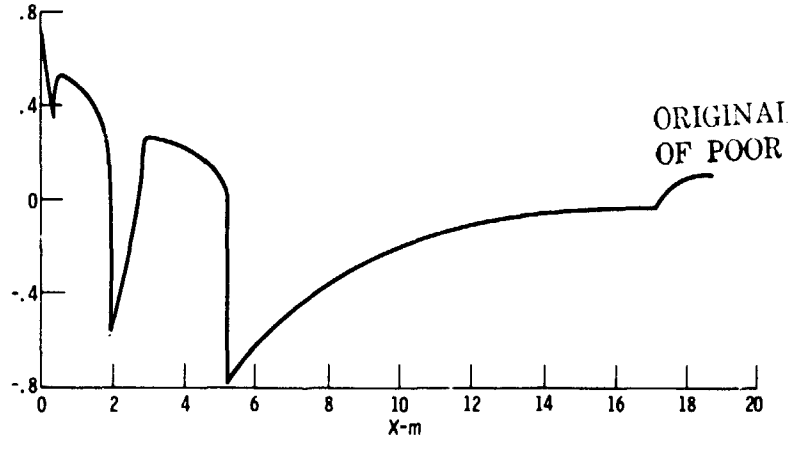




(c) Surface pressure coefficient vs distance along vehicle at $M_\infty = 1.0$.

Figure 3.

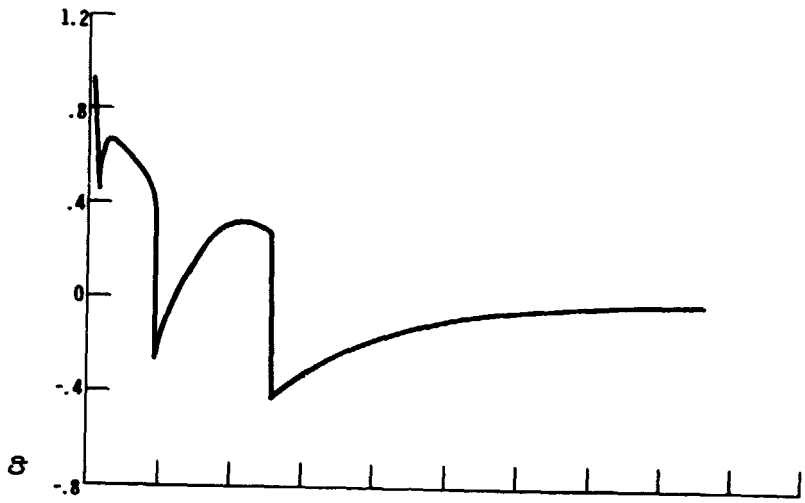


(d) Surface pressure coefficient vs distance along vehicle at $M_\infty = 1.2$.

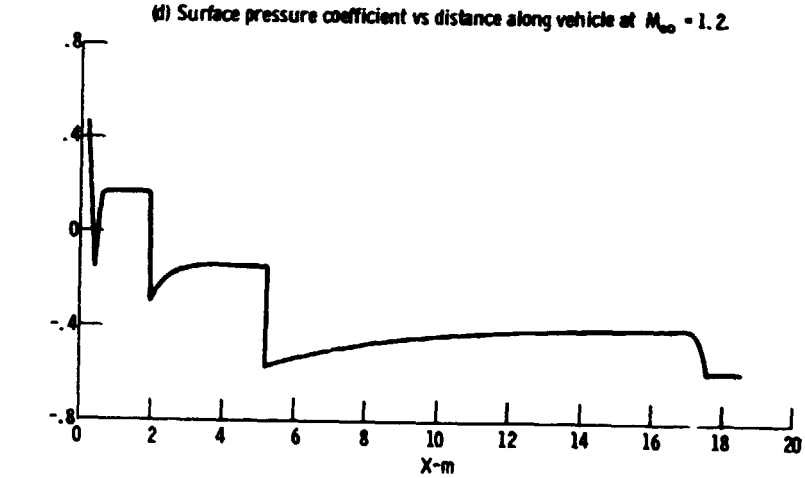


(e) Surface pressure coefficient vs distance along vehicle at $M_\infty = 1.56$.

Figure 3. - Concluded.

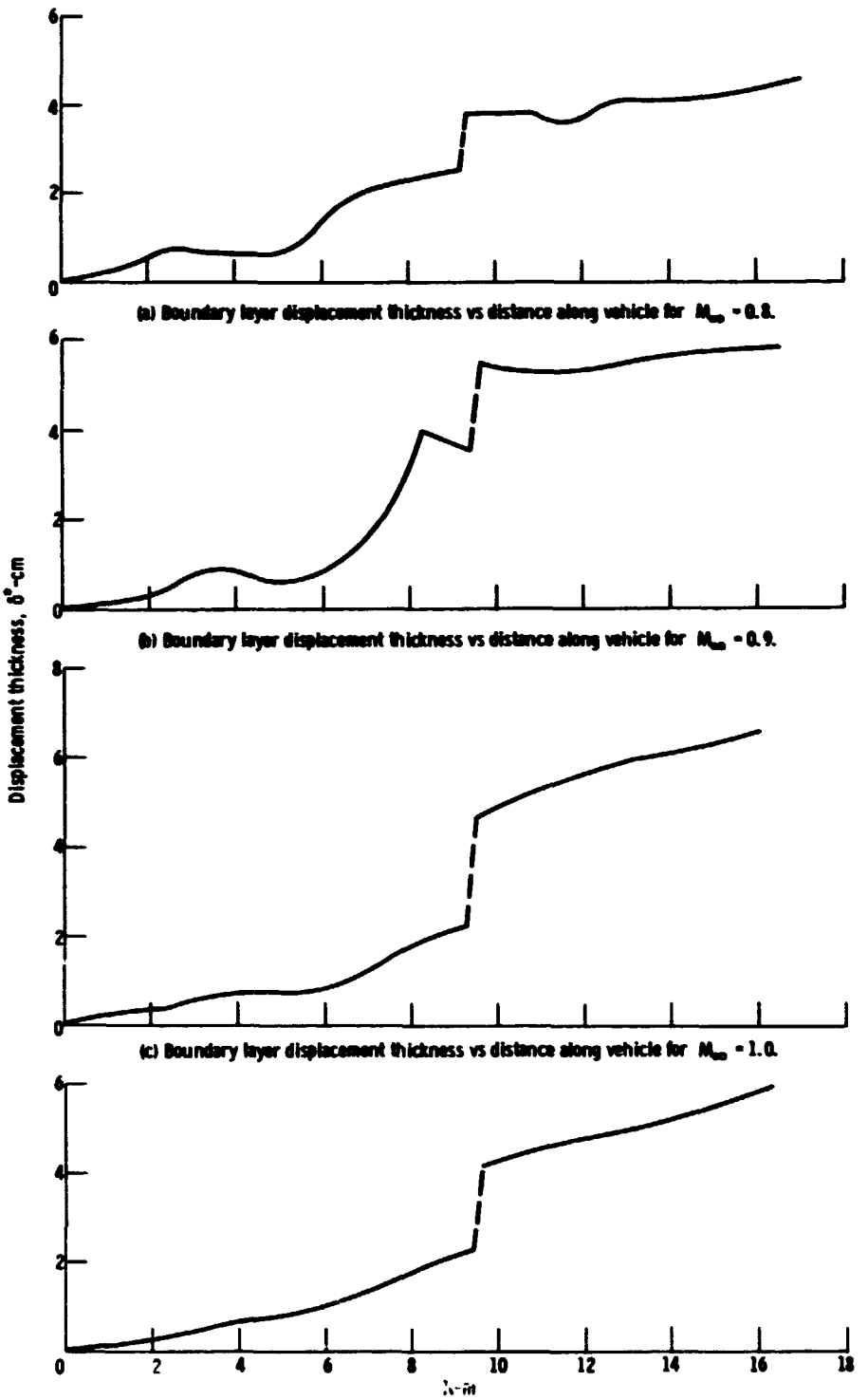


(a) Boundary layer displacement thickness vs distance along vehicle for $M_\infty = 0.8$.

(b) Boundary layer displacement thickness vs distance along vehicle for $M_\infty = 0.9$.

(c) Boundary layer displacement thickness vs distance along vehicle for $M_\infty = 1.0$.

(d) Boundary layer displacement thickness vs distance along vehicle for $M_\infty = 1.56$.

Figure 4.

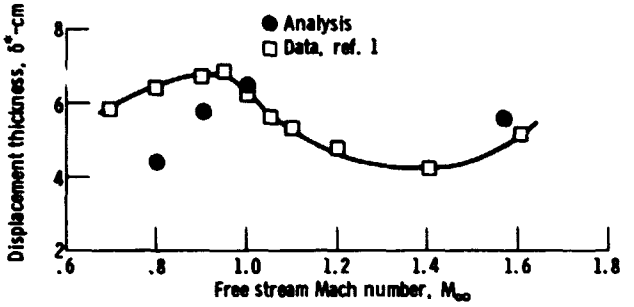


Figure 5. - Comparison of experimental and analytical displacement thicknesses downstream of the flange for various free stream Mach numbers.

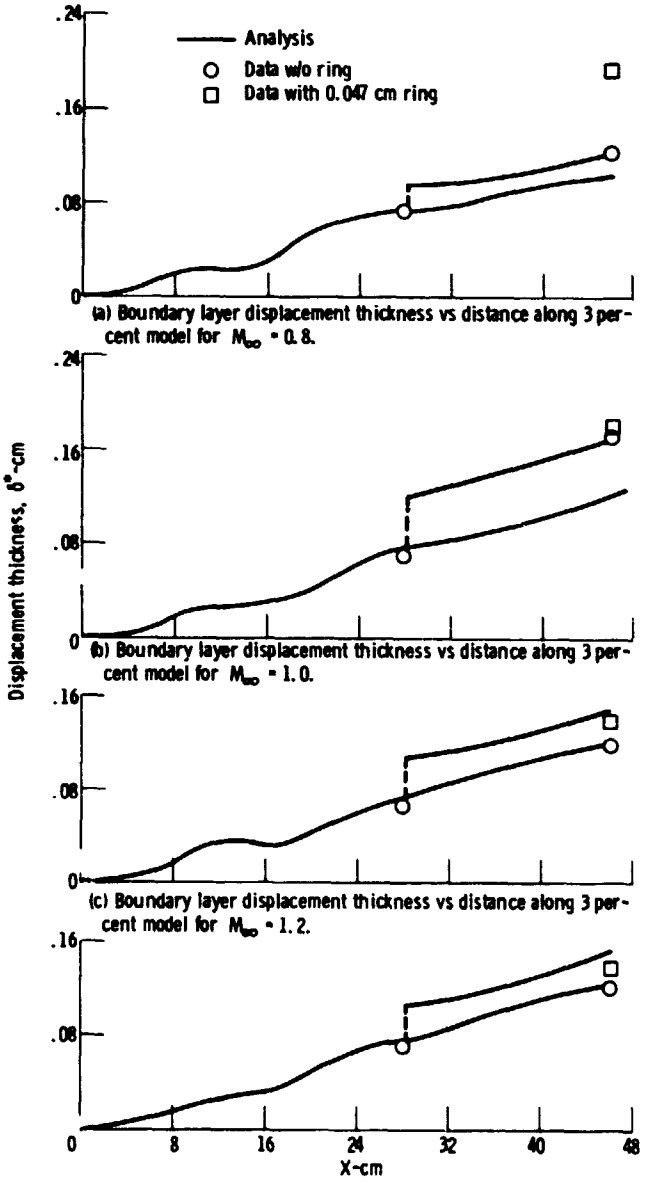


(a) Boundary layer displacement thickness vs distance along 3 percent model for $M_\infty = 0.8$.

(b) Boundary layer displacement thickness vs distance along 3 percent model for $M_\infty = 1.0$.

(c) Boundary layer displacement thickness vs distance along 3 percent model for $M_\infty = 1.2$.

(d) Boundary layer displacement thickness vs distance along 3 percent model for $M_\infty = 1.56$.

Figure 6.

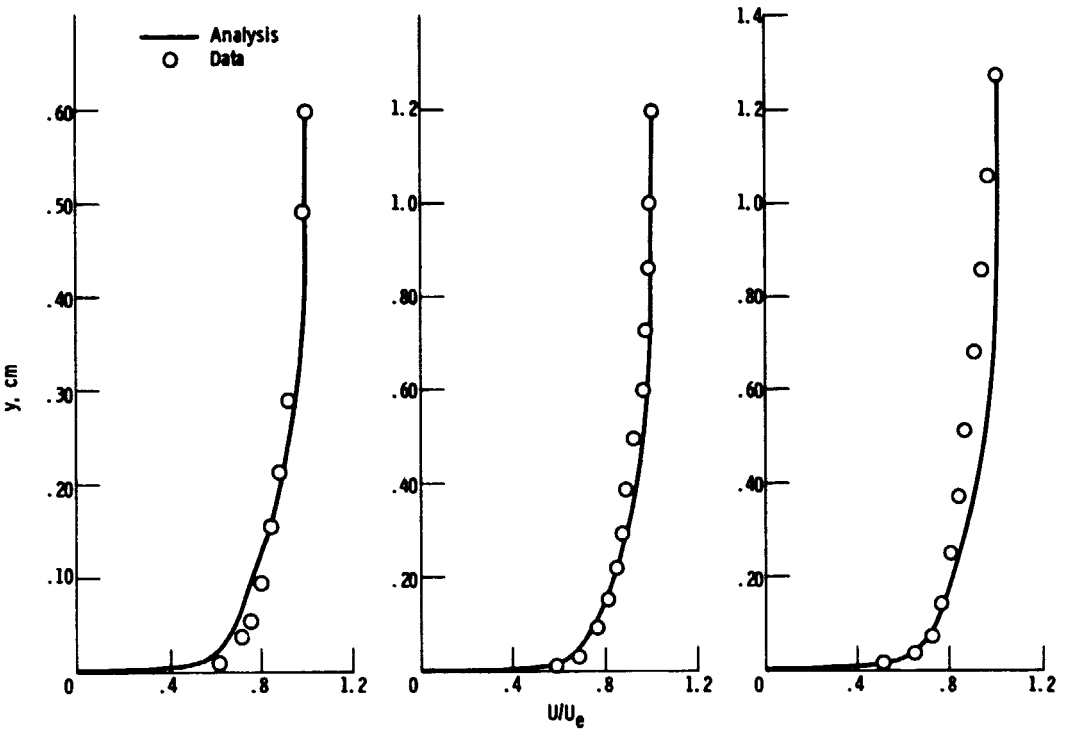


(a) Upstream profile. (b) Aft profile w/o ring. (c) Aft profile with ring.

Figure 7. - Boundary layer velocity profiles on 3 percent model for M = 0.8.

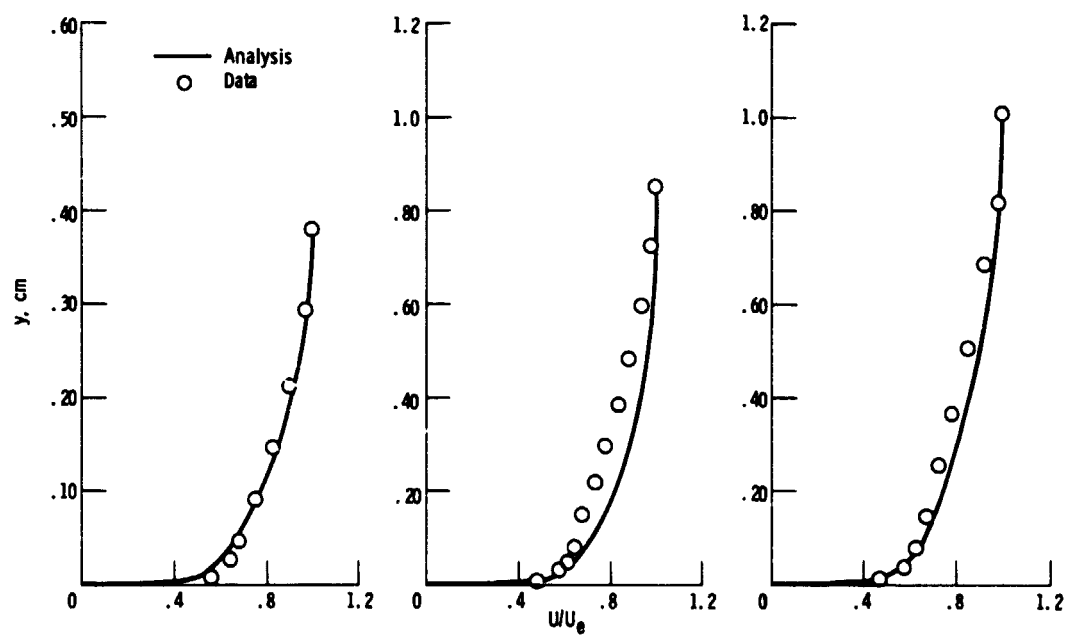


(a) Upstream profile. (b) Aft profile w/o ring. (c) Aft profile with ring.

Figure 8. - Boundary layer velocity profiles on 3 percent model for $M_\infty = 1.0$.

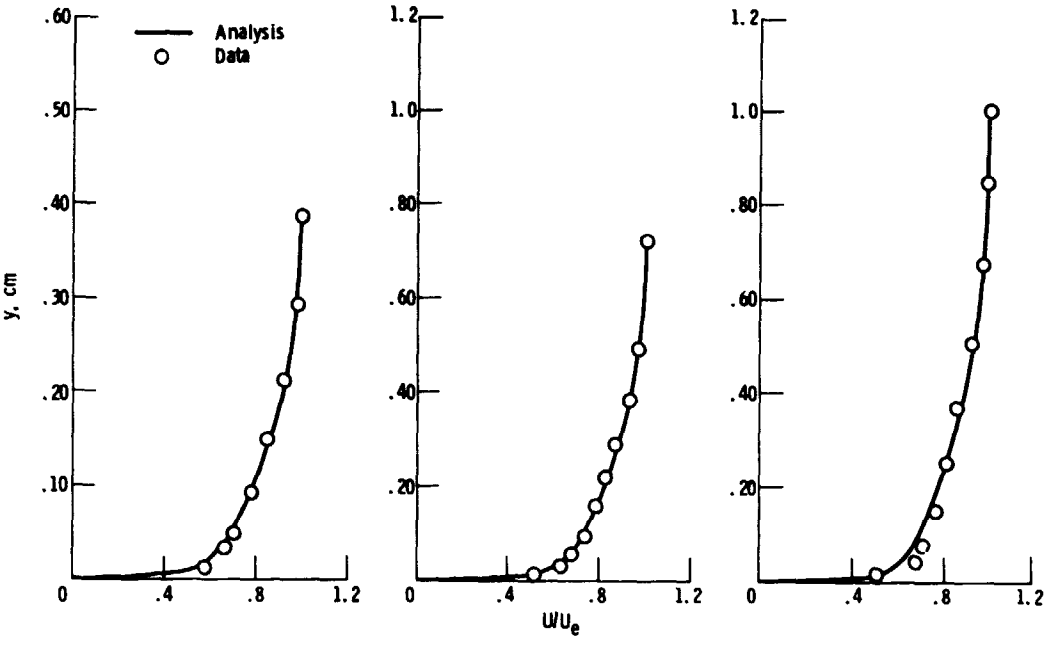


(a) Upstream profile. (b) Aft profile w/o ring. (c) Aft profile with ring.

Figure 9. - Boundary layer velocity profiles on 3 percent model for $M_{\infty} = 1.2$.

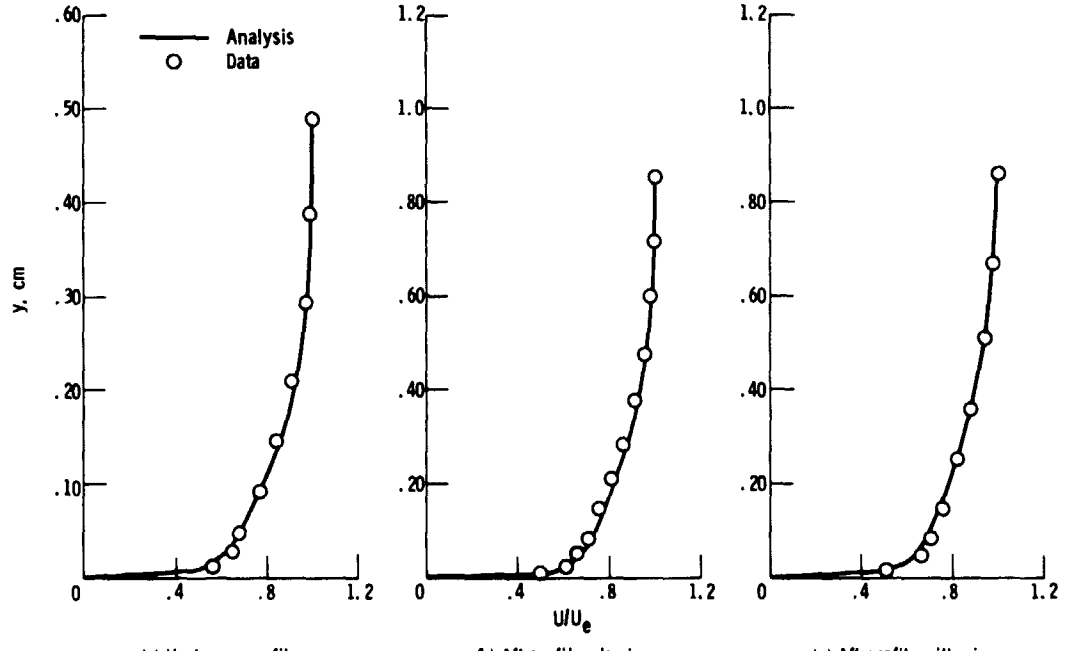


(a) Upstream profile. (b) Aft profile w/o ring. (c) Aft profile with ring.

Figure 10. - Boundary layer velocity profiles on 3 percent model for $M_{\infty} = 1.56$.